

ITC 2/52 Information Technology and Control Vol. 52 / No. 2 / 2023 pp. 515-528 DOI 10.5755/j01.itc.52.2.31649	A Novel Control Method for Unmanned Agricultural Tractors: Composite Back-stepping Sliding Mode Path Tracking	
	Received 2022/06/19	Accepted after revision 2023/01/30
	HOW TO CITE: Ji, X., Wei, X., Wang, A. (2023). A Novel Control Method for Unmanned Agricultural Tractors: Composite Back-stepping Sliding Mode Path Tracking. <i>Information Technology and Control</i> , 52(2), 515-528. https://doi.org/10.5755/j01.itc.52.2.31649	

A Novel Control Method for Unmanned Agricultural Tractors: Composite Back-stepping Sliding Mode Path Tracking

Xin Ji, Xinhua Wei, Anzhe Wang

College of Agricultural Engineering, Jiangsu University, Zhenjiang 212013, China

Corresponding author: wei_xh@163.com

A composite back-stepping sliding mode controller is proposed in the paper to address the under-actuated, input saturated, and time-varying disturbances, as well as model-dependent issues that bother the path tracking control of unmanned agricultural tractors. Specifically, the path tracking error model is introduced. The extended state observers (ESO) with time-varying parameters are employed to handle the lump disturbances resulting from the external disturbances and model nonlinearity. A novel composite path tracking controller is proposed based on back-stepping method, active disturbance rejection control, and sliding mode control, whose effectiveness is verified by theory analysis, simulations, and experiments. According to the results, the proposed controller outperforms the improved pure pursuit control in reducing the lateral offset.

KEYWORDS: Back-stepping sliding mode, Extended state observer, Path tracking control, Unmanned agricultural tractor.

1. Introduction

Unmanned tractors in agricultural operations has been gaining popularity thanks to their high accuracy, low labor cost, favorable efficiency, etc., but they may suffer from hypofunction under unstructured and challenging working environments [1]. The commonly-existing wheel sliding, which undermines accuracy and even safety, is a typical example [6]. Due to the difficulty in establishing the precision mathematical model of agricultural vehicles, mathematical model-based control methods are not effective enough. The path tracking control of unmanned farm vehicles remains to be a problem featuring serious nonlinearity, time-varying disturbances, and under-actuated characteristics [25].

The path tracking control of unmanned farm tractors generally serves as a guide for vehicles to follow the predetermined paths that cover the field, through which, the current lateral offset, heading offset, position information from position sensors, and attitude sensors are obtained [28]. The actuating components covering hydraulic valves [22] and electric steering wheels [16] are then adopted to control the vehicle steering angle via a specific algorithm. Besides, a series of methods have been explored for better performance of the precision tracking control. One representative is the model predictive control (MPC) proposed by Falcone et al. [5] to achieve trajectory tracking control when the vehicle is subject to kinematic, dynamic, and actuator restrictions. However, the optimal control requires hardware performance, especially in computing power. As a response, Fang et al. [6] designed a back-stepping controller that relieved the sliding effect through parameters adaption. However, such methods are generally based on an accurate model that is hard to establish in extreme environments, which complicates the design of a model-dependent vehicle controller because of the existing inevitable uncertain factors.

A model-free control method called Active Disturbance Rejection Control (ADRC) first proposed by Han [9] was inherited and developed by Gao [7]. After translating the actual model into an integral chain model, the disturbance observer, Extended State Observer (ESO), is adopted to determine the lump disturbance, guaranteeing its strong robustness and low reliance on the precise mathematical model. The

ADRC has been extensively used in diverse fields, including disturbance coupling control [27], spraying control [10], and unmanned aerial vehicles [26]. As for the ground vehicle path tracking control, Xia et al. [18] designed a lateral path tracking controller taking into account the ADRC and differential flatness theory. Chen et al. [3] later launched an improved linear active disturbance rejection control (LADRC) method. The sliding mode control (SMC) is an effective control theory that far outranks in parameter uncertainty, disturbance rejection, and finite-time convergence [14]. However, it also has flaws, covering the chattering phenomenon that is mainly derived from the discontinuous sign function and causes severe problems such as mechanical damage, shorter service life, and so on [12, 20], and its immunity to matched disturbance, that is, the disturbance and control input act on the same channel [8]. Because of the mismatched disturbance caused by unknown external disturbances and model nonlinearity in the path tracking control of unmanned tractors, the attenuation of the mismatched disturbance influence and the sliding mode controller chattering phenomenon are urgent issues to be addressed. Research on mismatched disturbance suppression is fruitful [4, 13], which supports the essential role of the combination of SMC and disturbance observer (i.e., composite SMC) in suppressing the chattering and disturbance. Wu et al. [17] constructed a robust control strategy to handle external disturbance using the terminal sliding model technology and ESO, but its costs are high as it uses extra sensors and state observers in estimating the slippage angle.

A composite back-stepping sliding mode controller is adopted for the path tracking control of unmanned tractors in the paper in response to such issues as model dependence and disturbance rejection, with the traditional path tracking problem translated into a second-order single-input and multiple-output model featuring nonlinearity, under-actuated characteristics, and unknown disturbances. Meanwhile, two time-varying parameters ESOs are taken to estimate the disturbances that exist in the lateral error subsystem and heading error subsystem, respectively, the latter of which is decoupled by the newly-introduced virtual heading angle control variable. The finite-time

reaching control law is also adopted to guarantee the sliding variable's finite-time convergence. Finally, the control expression of the front-wheel steering angle with hyperbolic tangent function saturation constraint is derived. The proposed scheme can effectively enhance the robustness and flexibility, lowering its reliance on the mathematical model. The major contributions of this paper can be summarized as follows:

- 1 Two ESO with time-varying parameters are introduced to estimate both lumped mismatched and matched disturbances. In this way, the peaking phenomenon with large initial error can be significantly reduced.
- 2 The composite back-stepping sliding mode control can significantly increase the system's robustness under different scenarios without having to rely on the precise mathematical model.
- 3 The power reaching law guarantees that the sliding variable can reach the designed sliding manifold in a finite time, and that the lateral offset can reach a bounded set around zero asymptotically with disturbances.

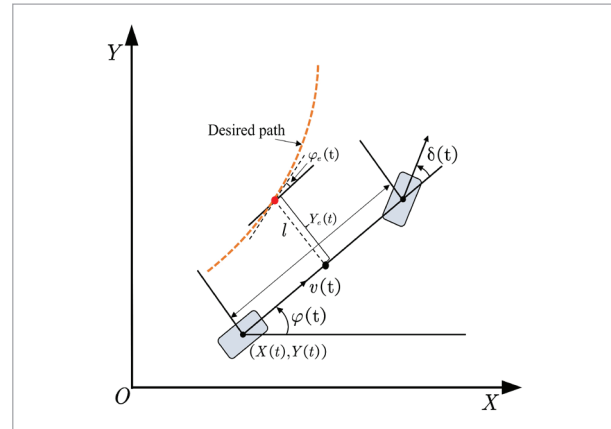
The rest of the paper is organized as follows. Section 2 describes the kinematic and error model of the unmanned tractor path tracking system in presence of matched and mismatched disturbances. Section 3 introduces the design of ESO and back-stepping SMC, respectively. Section 4 and Section 5 illustrate the simulation and experiments that prove the effectiveness and convergence of the proposed observer and controller. Section 6 concludes the manuscript.

2. Problem Formulation

The vehicle is assumed to be front-wheel steering and rear-wheel drive with constant speed in the absence of generality. Therefore, the tractor is simplified into 2 degrees of freedom (DOF) bicycle model that only considers the lateral movement. The application of such a model is commonly seen in many papers, as shown in Figure 1 [11, 15].

The coordinate system OXY refers to the inertial coordinate system fixed on the ground, while $(X(t), Y(t))$ the longitudinal and lateral displacements of the tractor in the ground. The motion model is described as follows:

Figure 1
Kinematic of the unmanned tractor



$$\begin{cases} \dot{X}(t) = v(t) \cos(\varphi(t)) \\ \dot{Y}(t) = v(t) \sin(\varphi(t)) \\ \dot{\varphi}(t) = \frac{v(t)}{l} \tan(\delta(t)) \end{cases}, \quad (1)$$

where $v(t)$ represents the longitudinal velocity that can be taken as the constant, l the wheelbase between the front wheel and the rear wheel, $\delta(t)$ the steering angle of the front wheel, and $\varphi(t)$ the heading angle.

The method frequently employed is the one that transforms the 2-DOF model into a small-angle approximation model and the nonlinear model into a linear model. Other approaches like a state feedback controller or backstepping controller are also adopted, which fail to handle the path tracking, especially under time-varying disturbances because of both its limited application around a small origin of the error and the asymptotical convergence characteristic of error.

The reference path falls into two categories, including straight-line paths and curve paths. Combined with kinematic constraints, the reference model is described as follows:

$$\begin{cases} \dot{X}_r(t) = v_r(t) \cos(\varphi_r(t)) \\ \dot{Y}_r(t) = v_r(t) \sin(\varphi_r(t)) \\ \dot{\varphi}_r(t) = \frac{v_r(t)}{l} \tan(\delta_r(t)) \end{cases}, \quad (2)$$

where the subscript r denotes the reference model.

Considering the difference between the system (1) and (2), the error model is

$$\begin{bmatrix} X_e(t) \\ Y_e(t) \\ \varphi_e(t) \end{bmatrix} = \begin{bmatrix} \cos(\varphi(t)) & \sin(\varphi(t)) & 0 \\ -\sin(\varphi(t)) & \cos(\varphi(t)) & 0 \\ 0 & 0 & 1 \end{bmatrix} \begin{bmatrix} X_r(t) - X(t) \\ Y_r(t) - Y(t) \\ \varphi_r(t) - \varphi(t) \end{bmatrix}, \quad (3)$$

where the subscript e stands for the error model. The differentiation of the error model (3) leads to

$$\begin{cases} \dot{X}_e(t) = \dot{\varphi}(t)Y_e(t) - v(t) + v_r(t)\cos(\varphi_e(t)) \\ \dot{Y}_e(t) = v_r(t)\sin(\varphi_e(t)) - \dot{\varphi}(t)X_e(t) \\ \dot{\varphi}_e(t) = \frac{v_r(t)}{l}\tan(\delta_r(t)) - \frac{v(t)}{l}\tan(\delta(t)) \end{cases}, \quad (4)$$

The error system is transformed into a second-order system with the longitudinal motion neglected

$$\begin{cases} \dot{Y}_e(t) = v_r(t)\sin(\varphi_e(t)) - \dot{\varphi}(t)X_e(t) \\ \dot{\varphi}_e(t) = \frac{v_r(t)}{l}\tan(\delta_r(t)) - \frac{v(t)}{l}\tan(\delta(t)) \end{cases}. \quad (5)$$

Taking into account the natural decoupling feature of ESO, the error model can be depicted as follows

$$\begin{cases} \dot{Y}_e(t) = \varphi_e(t) + v_r(t)\sin(\varphi_e(t)) - \varphi_e(t) - \dot{\varphi}(t)X_e(t) \\ \dot{\varphi}_e(t) = -\frac{v(t)}{l}\tan(\delta(t)) + \frac{v_r(t)}{l}\tan(\delta_r(t)) \end{cases}. \quad (6)$$

The modeling deviations, external disturbances, and the system nonlinearities are taken as the lump disturbances, while the state variables and control input are selected as $Y_e(t)$, $\varphi_e(t)$ and $u = \tan(\delta(t))$, respectively. Finally, system (6) is converted into

$$\begin{cases} \dot{Y}_e(t) = \varphi_e(t) + d_1; \quad \dot{\varphi}_e(t) = b_0u(t) + d_2 \\ |u(t)| \leq \tan(\delta_{\max}) \end{cases}, \quad (7)$$

where $d_1 = v_r(t)\sin(\varphi_e(t)) - \varphi_e(t) - \dot{\varphi}(t)X_e(t) + w_1(t)$; $d_2 = v_r(t)/l\tan(\delta_r(t)) + w_2(t) + \Delta b \cdot u$; $b_0 = -v(t)/l$; Δb represents the model parameter uncertainty, δ_{\max} the maximum front-wheel steering angle, d_1 and d_2 the lumped mismatched disturbance and the lumped matched disturbance in lateral deviation and heading deviation, respectively, while $w_1(t)$ and $w_2(t)$ the external disturbances generally caused by the road surface, wheel slips, and so on. The matched and mismatched disturbances and their derivatives are as-

sumed to be bounded with the absence of generality.

$$|d_i| \leq \tau_i, \quad |\dot{d}_i| \leq \varrho_i, \quad i = 1, 2, \quad (8)$$

where $\tau_i > 0$ and $\varrho_i > 0$ are constants. d_i is defined to contain the system's nonlinearities and external disturbances. For instance, the system nonlinearities are bounded owing to their interdependence on the bounded states.

Remark 1. The external disturbances that reflect the form of velocities like sliding are far less than the linear velocity based on the dynamic analysis of the vehicle, which supports their bounded relationship.

3. Path Tracking Controller Design

The following notations are predetermined before the controller design. The signum function is defined as the following:

$$\text{sign}(x) = \begin{cases} 1 & x > 0 \\ 0 & x = 0 \\ -1 & x < 0 \end{cases}$$

The fractional power is defined as follows for simplicity:

$$\text{sgn}(x)^r = \text{sign}(x) |x|^r.$$

3.1. Extended State Observer Design

2 ESOs are designed to estimate the disturbances in the lateral subsystem and heading subsystem, respectively, thus bettering the performance of tracking and disturbance rejection. The system (7) is firstly decomposed into two subsystems, including lateral and heading subsystems. Two other extended subsystems are obtained thanks to the introduction of the extended state variables.

$$\text{Subsys 1: } \begin{cases} \dot{Y}_e(t) = \varphi_e(t) + x_{11}; \quad \dot{x}_{11} = f_1 \end{cases}, \quad (9)$$

$$\text{Subsys 2: } \begin{cases} \dot{\varphi}_e(t) = b_0u(t) + x_{12}; \quad \dot{x}_{12} = f_2 \end{cases},$$

where $x_{11} = d_1$, $\dot{d}_1 = f_1$, $x_{12} = d_2$, $\dot{d}_2 = f_2$. Then, the time-varying parameters ESOs for the system (9) are constructed:

$$\text{ESO 1: } \begin{cases} \dot{\hat{Y}}_e(t) = \varphi_e(t) + \hat{x}_{11} - l_{11}e_1; \quad \dot{\hat{x}}_{11} = -l_{12}\tanh(\varepsilon e_1) \end{cases}, \quad (10)$$

$$\text{ESO 2: } \begin{cases} \dot{\hat{\varphi}}_e(t) = b_0u(t) + \hat{x}_{12} - l_{21}e_2; \quad \dot{\hat{x}}_{12} = -l_{22}\tanh(\varepsilon e_2) \end{cases},$$

where $l_{ij} > 0$, $i = 1, 2$, $j = 1, 2$ are observer gains, and $\varepsilon > 0$ denotes the change rate of observer error, $\hat{Y}_e(t)$ and $\hat{\varphi}_e(t)$ the estimations of $Y_e(t)$ and $\varphi_e(t)$, \hat{x}_{11} and \hat{x}_{12} the estimations of disturbances, while \tanh the hyperbolic tangent function. $e_1 = Y_e(t) - \hat{Y}_e(t)$, and $e_2 = \varphi_e(t) - \hat{\varphi}_e(t)$.

ESO serves as the key to ADRC. The initial nonlinear ESO designed by Han includes multiple parameters that require adjustment [9]. Gao developed a linear ESO (LESO) based on the concept of “bandwidth” [7]. The ESO or LESO peaks when the initial value has a large error, which can be explained by its nature as a high gain observer. Therefore, this paper designs time-varying parameters ESOs, where the time-varying parameters \tilde{l}_{11} and \tilde{l}_{12} will take the place of l_{11} and l_{12} according to the saturation characteristics of the hyperbolic tangent function. The time-varying parameters are designed as

$$\begin{aligned} \tilde{l}_{11} &= l_{11} \tanh(b_1 t), \\ \tilde{l}_{12} &= l_{12} \tanh(b_2 t), \end{aligned} \tag{11}$$

where t stands for the running time, while b_1 and b_2 denote the change rate of control parameters. The same goes for the design of the heading subsystem.

3.2. Back-stepping Sliding Mode Controller Design

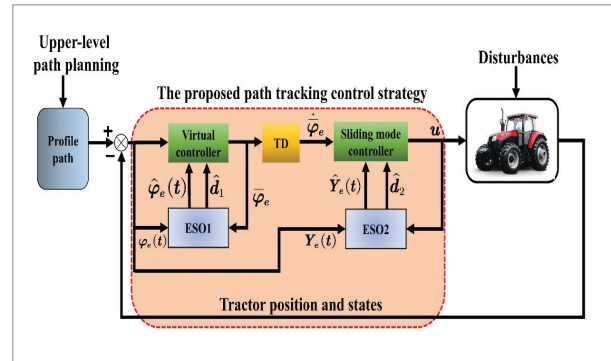
Figure 2 reveals the proposed composite control scheme that covers two ESOs, the virtual heading controller, the sliding mode controller.

It should be pointed out that noises such as external environment noises, sensor noises, etc. widely exist in the path tracking system. The direct differential exact method will enlarge the noises. In order to exact the differential signal under noises, the tracking differential (TD) is employed, as can be found from Han’s work [9].

The core technology of the back-stepping controller is a step-by-step construction. The stabilization of the former subsystem cannot be realized without the virtual control of the latter subsystem. In lateral subsystem, φ_e is taken as a virtual control, whose quantity is required to both stabilize the system and reject the disturbance. As a result, the heading angle virtual controller can be described as follows, considering the idea of ADRC.

Figure 2

Path tracking control scheme of the unmanned tractor



$$\bar{\varphi}_e(t) = -\lambda_Y Y_e(t) - \hat{x}_{11}, \tag{12}$$

where λ_Y serves as a positive controller parameter.

The virtual control $\bar{\varphi}_e$ can ensure the lateral deviation converge to zero or a residual set around zero asymptotically. The sliding mode controller proposed by Yu et al. is adopted in the paper with the heading deviation φ_e tracking the desired virtual control input [23]. The sliding surface is calculated with $\sigma = \varphi_e - \bar{\varphi}_e$

$$s = \sigma = \varphi_e - \bar{\varphi}_e. \tag{13}$$

A reaching control law is constructed as follows to guarantee the gathering of sliding variables to the sliding manifold in a finite time.

$$\dot{s} = -ps - q \operatorname{sgn}(s)^r, \tag{14}$$

where $p > 0$, $q > 0$, $0 < r < 1$. The equation (14) outperforms the traditional reaching control law in ensuring the reaching of the sliding variable to the sliding manifold in a finite time and in reducing the chattering phenomenon by adjusting the parameters.

Yields are expressed as follows considering the derivative of equation (13)

$$\dot{s} = \dot{\varphi}_e - \dot{\bar{\varphi}}_e. \tag{15}$$

The sliding mode controller is designed as

$$u(t) = b_0^{-1} \left(\dot{\bar{\varphi}}_e - \dot{x}_{12} - ps - q \operatorname{sgn}(s)^r \right). \tag{16}$$

The application of the x_{12} estimated from Equations (10) into (16) helps rewrite the controller.

$$u(t) = b_0^{-1} (\dot{\varphi}_e - \hat{x}_{12} - ps - q \operatorname{sgn}(s)^r). \quad (17)$$

The controller (16), which combines the advantages of the following works [16, 17, 24], successively decouples the under-actuated characteristic and estimates the disturbances combined with ESOs, exhibiting better dynamic performance than Wang et al.'s [15] work when combined with SMC. The lateral deviation serves as the main concern and the heading virtual control is adopted to adjust the lateral deviation in the presence of mismatched disturbance, which shares the idea of [17]. However, controller (16) requires no additional sensors to explore the sliding effect, which sets itself apart from Wu et al.'s work [17]. The front-wheel angle is limited during the actual control process. Similarly, the bounded hyperbolic tangent function is used to limit the control input that is expressed as follows

$$\delta = \arctan \left(N \tanh \left(\frac{\dot{\varphi}_e - \hat{x}_{12} - ps - q \operatorname{sgn}(s)^r}{Nb_0} \right) \right), \quad (18)$$

where N represents the maximum front-wheel angle of the actual tractor. The hyperbolic tangent function is also taken as a substitute to the sign function to relieve the chattering problem [2].

Theorem 1. The lateral deviation will converge into a bounded set under the observers (10), and controller (17) with suitable parameters.

Proof. The proof of Theorem 1 will be divided into three steps. Primarily, the boundness of the estimated error will be proved.

Step 1. First, the boundness of observer errors will be proved. To simplify the proving process, the proof of the lateral subsystem is given. Defining estimation error $e_d = x_{11} - \hat{x}_{11}$, and let $z_1 = e_1$, $z_2 = -e_d - l_{11}e_1$. Combining with (9) and (10), it shows that

$$\begin{cases} \dot{z}_1 = z_2 \\ \dot{z}_2 = -l_{12} \tanh(\varepsilon z_1) - l_{11} z_2 - f_1 \end{cases} \quad (19)$$

Choosing the Lyapunov candidate function as

$$L_z = l_{12} \int_0^{z_1} \tanh(\varepsilon z_1) dz_1 + \frac{1}{2} z_2^2. \quad (20)$$

Taking the derivate of (20), combing it with (19) and (9), it can conclude that

$$\begin{aligned} \dot{L}_z &= l_{12} \tanh(\varepsilon z_1) z_2 + z_2 \dot{z}_2 \\ &= l_{12} \tanh(\varepsilon z_1) z_2 + z_2 (-l_{12} \tanh(\varepsilon z_1) - l_{11} z_2 - f_1) \\ &= -z_2 (f_1 + l_{11} z_2) \\ &= -l_{11} \left(z_2 + \frac{f_1}{2l_{11}} \right)^2 + \frac{f_1^2}{4l_{11}} \\ &\leq -l_{11} \left(z_2 + \frac{f_1}{2l_{11}} \right)^2 + \frac{q_1^2}{4l_{11}}. \end{aligned} \quad (21)$$

It can be seen from (21) that z_1 and z_2 are bounded. When $|z_2| \leq \frac{q_1}{l_{11}}$, the system is stable. From (19), when the system reached the stable, one can obtain that

$$\dot{z}_2 = -l_{12} \tanh(\varepsilon z_1) - l_{11} z_2 - f_1 = 0. \quad (22)$$

According to the monotone increasing characteristic of the hyperbolic tangent function, hence we have $|z_1| \leq \frac{1}{\varepsilon} \tanh^{-1} \left(\frac{2q_1}{l_{12}} \right)$. Finally, the observer errors are bounded as

$$\begin{aligned} \sup(e_1) &= \frac{1}{\varepsilon} \tanh^{-1} \left(\frac{2q_1}{l_{12}} \right), \\ \sup(e_d) &= \frac{q_1}{l_{11}} + \frac{l_{11}}{\varepsilon} \tanh^{-1} \left(\frac{2q_1}{l_{12}} \right), \end{aligned} \quad (23)$$

it shows that the observer errors are bounded.

Step 2. Next, the convergence of the sliding variable s will be proved. Choosing the Lyapunov candidate function as

$$L_s = \frac{1}{2} s^2. \quad (24)$$

According to (24), and we have $2L_s = s^2 = \|s\|^2$ and $2^{(r+1)/2} L_s^{(r+1)/2} = 2^{(r+1)/2} \left(\frac{1}{2} s^2 \right)^{(r+1)/2} = |s|^{r+1}$. Taking the derivate of (24), combining the controller (17) and (14), we have

$$\begin{aligned} \dot{L}_s &= s\dot{s} = s(b_0 u + x_{12} - \dot{\varphi}_e) \\ &= s(-ps - q \operatorname{sgn}(s)^r + x_{12} - \hat{x}_{12}) \\ &\leq -p_{\min} \|s\|^2 - q_{\min} |s|^{r+1} - se_m \\ &\leq -2p_{\min} L_s - 2^{(r+1)/2} q_{\min} L_s^{(r+1)/2} - se_m, \end{aligned} \quad (25)$$

where $e_m = x_{12} - \hat{x}_{12}$; $p_{\min} = p - \mu_1$ and $q_{\min} = q - \mu_2$; $0 < \mu_1 < p$ and $0 < \mu_2 < q$ are positive infinitesimal.

From (25), it can conclude that if the controller parameters can be selected large enough such that $\dot{L}_s < 0$ when L_s is out of a certain bounded region. The sliding variable will be guaranteed to a close neighborhood of the sliding manifold in a finite time [24-26], and the sliding variable is bounded ultimately as

$$s \in (\|s\| \leq \|e_m\|/p_{\min}) \cap (|s| \leq (\|e_m\|/q_{\min})^{1/r}). \tag{26}$$

Step 3. To prove the convergence of lateral offset, taking the virtual control (12) into the lateral subsystem, we have

$$\dot{Y}_e(t) = \varphi_e(t) - \bar{\varphi}_e(t) - \lambda_Y Y_e(t) + x_{11} - \hat{x}_{11}. \tag{27}$$

According to Step 1, there exist positive constants C_φ and C_{11} such that

$$|\varphi_e - \bar{\varphi}_e| < C_\varphi \text{ and } |x_{11} - \hat{x}_{11}| < C_{11}. \tag{28}$$

For the lateral subsystem, it shows that

$$\dot{Y}_e(t) = -\lambda_Y Y_e(t) + C_\varphi + C_{11}. \tag{29}$$

Integrating (27) and combining with the *Gronwall-Bellman* inequality, yields

$$\begin{aligned} Y_e(t) &\leq (C_{11} + C_\varphi)t + Y_e(0) - \int_0^t \lambda_Y Y_e(\tau) d\tau \\ &\leq (C_{11} + C_\varphi)t + Y_e(0) - \int_0^t ((C_{11} + C_\varphi)\tau + Y_e(0))\lambda_Y \exp\left[\int_\tau^t (-\lambda_Y) d\gamma\right] d\tau \\ &\leq \frac{(C_{11} + C_\varphi)}{\lambda_Y} + Y_e(0)e^{-\lambda_Y t}, \end{aligned} \tag{30}$$

where $Y_e(0)$ is the initial lateral offset. Finally, the lateral deviation converges into a bounded set. It can be concluded from Step 1-3 that the sliding variable will reach the sliding surface in a finite time, and then the lateral offset will converge into a bounded set around zero.

4. Simulation Analysis of the Path Tracking Control System

Simulations of the back-stepping sliding mode controller are constructed in this section to illustrate the

effectiveness of the proposed controller. Matlab2018 is employed as the simulation platform and the Euler method as a tool to discrete the model and the controller. The simulation time is set as 25 s and the fixed step size is 0.001 s. Table 1 lists the relevant tractor parameters, observers gains, and controller parameters.

Table 1
Main parameters in controller (18)

Simulation parameters		
$l_{11} = 20$	$b_0 = -1$	$p = 3.5$
$l_{12} = 1200$	$b_1 = 65$	$r = 0.1$
$l_{21} = 20$	$b_2 = 65$	$q = 1.1$
$l_{22} = 1200$	$\lambda_Y = 2.5$	

The initial system states are $[Y_e(0) \ \varphi_e(0)] = [2 \ -1.5]$, and $\delta_{\max} = 30^\circ$. The back-stepping controller designed by [6] is adopted for comparison.

In order to test the proposed controller under different scenarios, the following three different cases are set. To simulate the sensor noises, environment noises, etc., the Gaussian white noise has been added in the simulations, as shown in Figure 3.

$$\begin{cases} \text{case1: } d_1 = 0.5 \sin(t), \\ \quad \quad \quad d_2 = 2.0 \sin(\cos(t)) + 0.05 \sin(t) \cdot u + \text{noise}, \\ \text{case2: } d_1 = 0.5 \sin(0.5t), \\ \quad \quad \quad d_2 = 2.0 \sin(\cos(0.5t)) + 0.05 \sin(2t) \cdot u + \text{noise}, \\ \text{case3: } d_1 = 0.5 \text{sign}(\sin(0.5t)), \\ \quad \quad \quad d_2 = 2.0 \text{sign}(\cos(0.5t)) + 0.05 \text{sign}(\cos(0.5t)) \cdot u + \text{noise}. \end{cases} \tag{30}$$

A simulation comparison between time-varying ESO and LESO is conducted to show the peak suppression of time-varying parameters ESO (Figure 3).

Figure 3 illustrates the observation value of disturbance. Both observers can track the given disturbance after 0.4s, while the ESO excels in suppressing the peaking phenomenon, performing smaller tracking errors, and tracking speed.

Figure 4 reveals the evolution of absolute lateral error of 2 controllers under three cases. The tractor performs absolute mean steady lateral error of 0.0989,

Figure 3
The history of LESO, time-varying parameters ESO and Gaussian noises

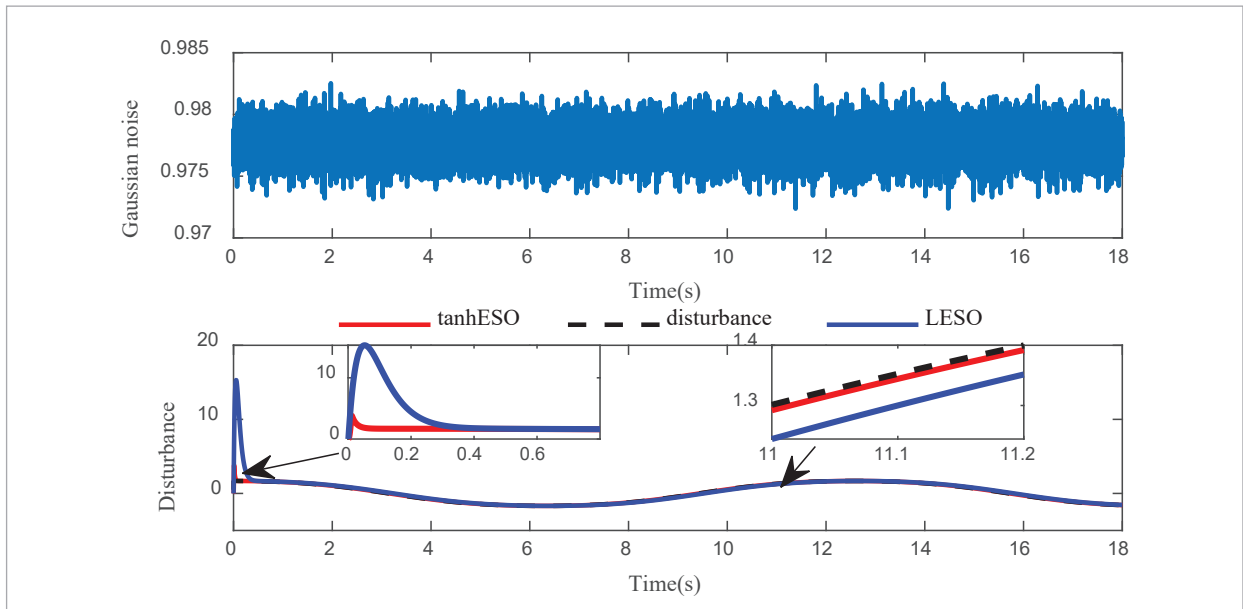


Figure 4
The absolute lateral offset under different speeds

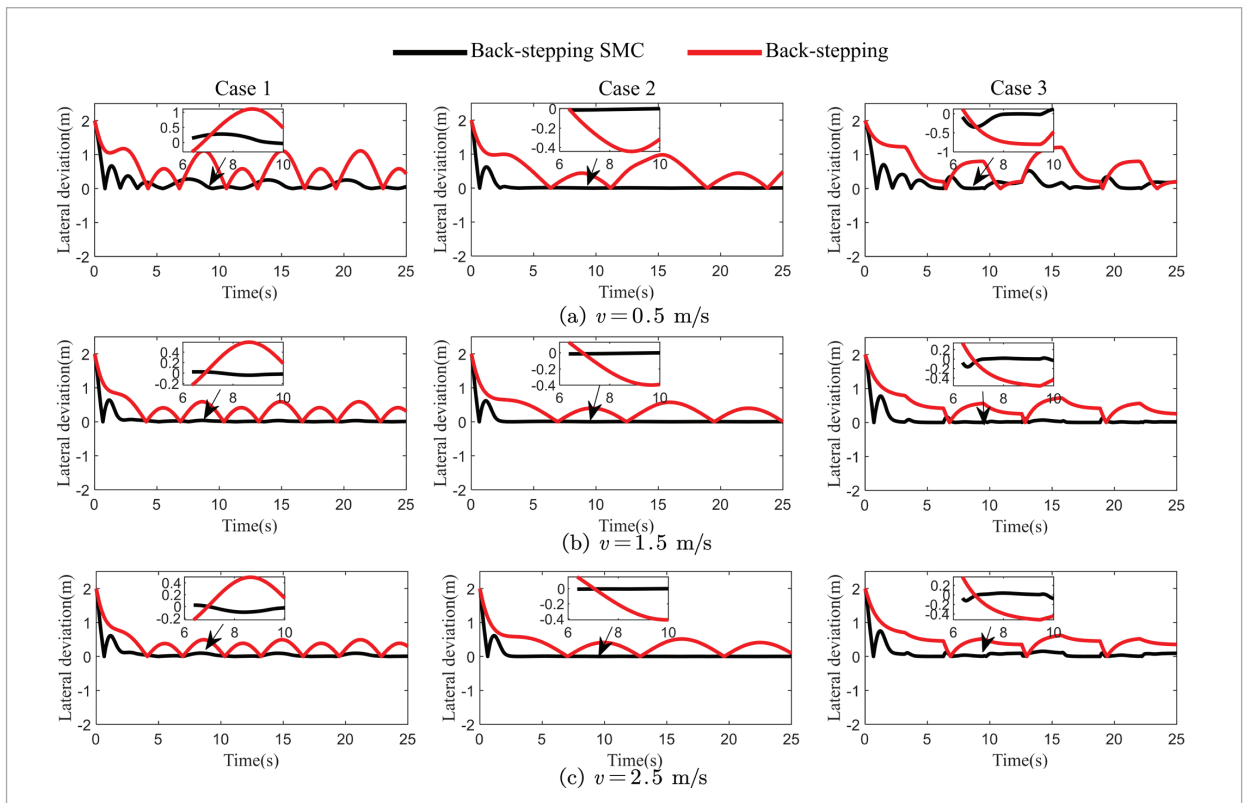
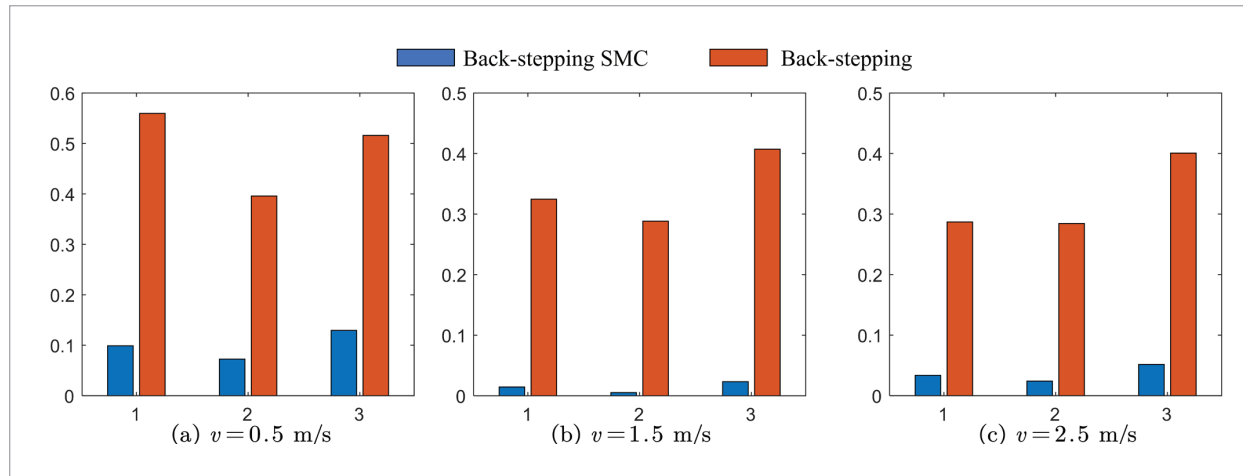


Figure 5

The mean absolute value of the steady lateral offset



0.0145, and 0.0336 after 3.17s, and the absolute mean steady lateral error of 0.5595, 0.3247, and 0.2869 after 3.71s with speeds of 0.5, 1.5, and 2.5 m/s, respectively, under the back-stepping SMC method in Case 1. The other two situations can be found in Figure 5. It can be concluded that, compared with the traditional controllers, the proposed controller can largely enhance the tracking accuracy under diverse speeds and disturbances.

5. Field Experiment Research

The field experiment research is conducted in Chongming Land (Shanghai, China) in November with a tractor (Dongfanghong, 1104) serving as the field test platform after relevant intelligent modification. This paper takes the 32-bit chip STM32 (TI Corporation, USA) as the vehicle controller, the electrical steering wheel (Lianshi Co., Ltd., Shanghai) as an alternative to the previous manned wheel, together with the angle sensor (Tianhaike Co., Ltd., Beijing) to measure the front steering's angle. The satellite positioning system (Beidou Xingtong Technology Co., Ltd., Beijing) and MTI-300 inertial navigation system (XS-ENS, Netherlands) also make contributions. Figure 6 portrays the experimental prototype.

The paper employs the pure pursuit controller frequently seen in unmanned tractors to compare the proposed controller and the back-stepping sliding

mode controller, thus verifying the former's actual effectiveness. The specific control input is

$$\delta = \arctan \frac{2l(Y \cos \varphi_e - \sqrt{L_d^2 - Y_e^2} \sin(\varphi_e))}{L_d^2}, \quad (32)$$

where L_d denotes the look-ahead distance.

Given the dependence of the control performance of the pure pursuit controller on the look-ahead distance, a fuzzy method is adopted in the paper to determine the optimal look-ahead distance that guarantees fairness [21, 23]. Besides, the lateral deviation and heading deviation act as the input, while the dynamic look-ahead distance is the output, which is subject to the following fuzzy rules.

- 1 The lateral deviation fuzzy set is {LV, LB, LM, LS, M, RS, RM, RB, RV};
- 2 The heading deviation fuzzy set is {LB, LM, LS, M, RS, RM, RB};
- 3 The look-ahead distance fuzzy set is {VC, C, LC, M, L, F, VF}.

This paper also employs the trigonometric membership function and the Mamdani method, the former of which is illustrated in Figure 7.

The test field consists of weeds and water accumulation, which leads to the sliding effect and external disturbance. Four boundary points (A, B, C, D) of the

Figure 6

Field experiment platform

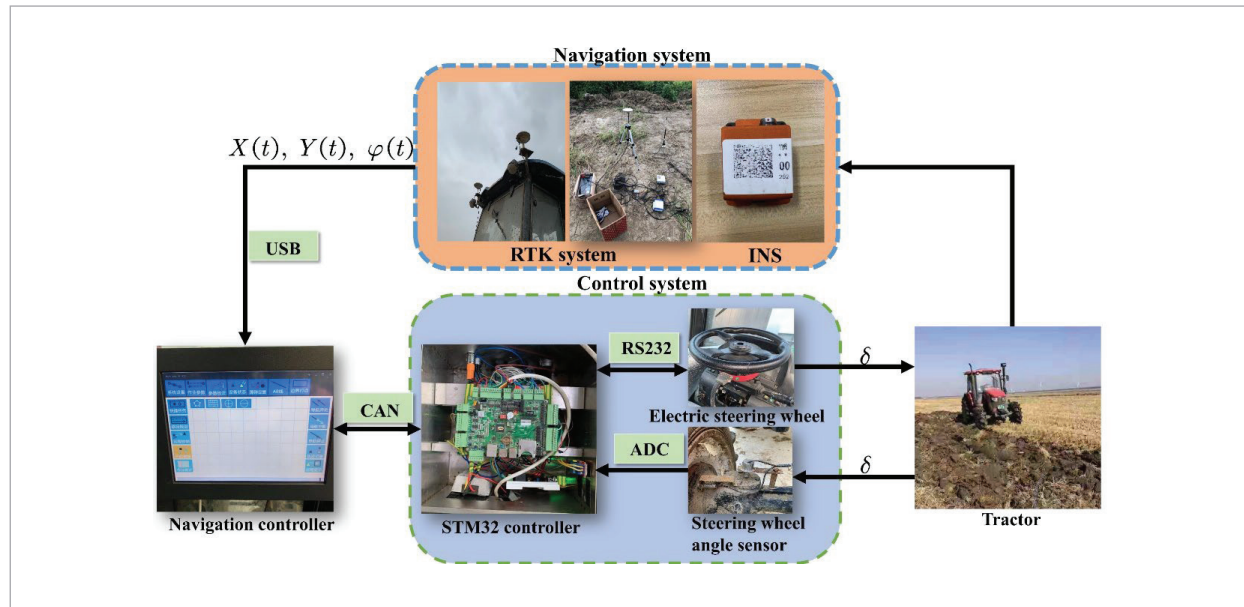
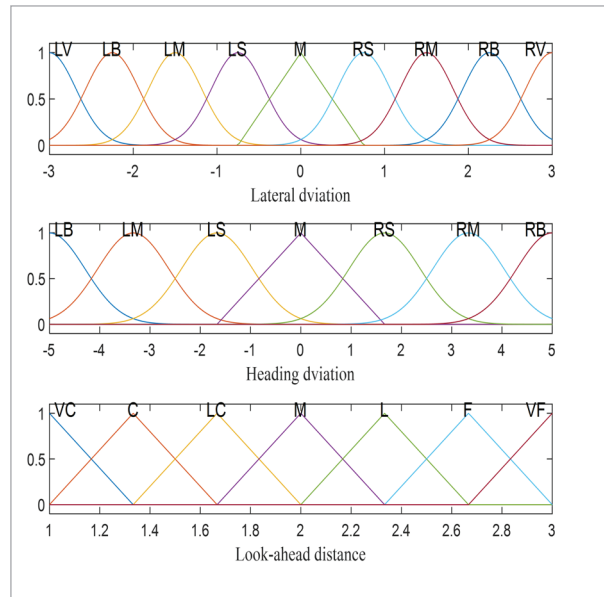


Figure 7

Sketches of membership functions



operation area are picked in a rectangular paddy field with a portable positioning receiver, and the reference path that includes the straight path and curve path is generated by the navigation controller that records the actual position, lateral deviation, and

heading angle deviation. The vehicle speed is fixed to be 1 m/s, the initial lateral deviation 0.3 m, while the initial heading angle deviation 0. Figure 8 reveals the reference path and the actual trajectories under the action of the two controllers.

Figure 9, Table 2, and Table 3 list the results of the proposed back-stepping SMC and the fuzzy pure pursuit control, according to which, the obvious lateral deviation of the fuzzy pure pursuit control are observed, especially in the curve path. The sliding effect that results in the time-varying disturbances to the tractor matters a lot during the turning operation. However, the design of the fuzzy pure pursuit control fails to consider the robustness.

The actuator that traps in a saturation dead zone undermines the dynamic response performance. As for the fuzzy pure pursuit control method, the minimum lateral deviation is 0.17 m during the straight path, while the maximum lateral deviation records 0.27 m during the curve path. The proposed controller performs favorably thanks to the disturbance observer and sliding mode control, and the lateral deviation is always within 0.045 m regardless of the path.

Figure 8
Field experiment paths

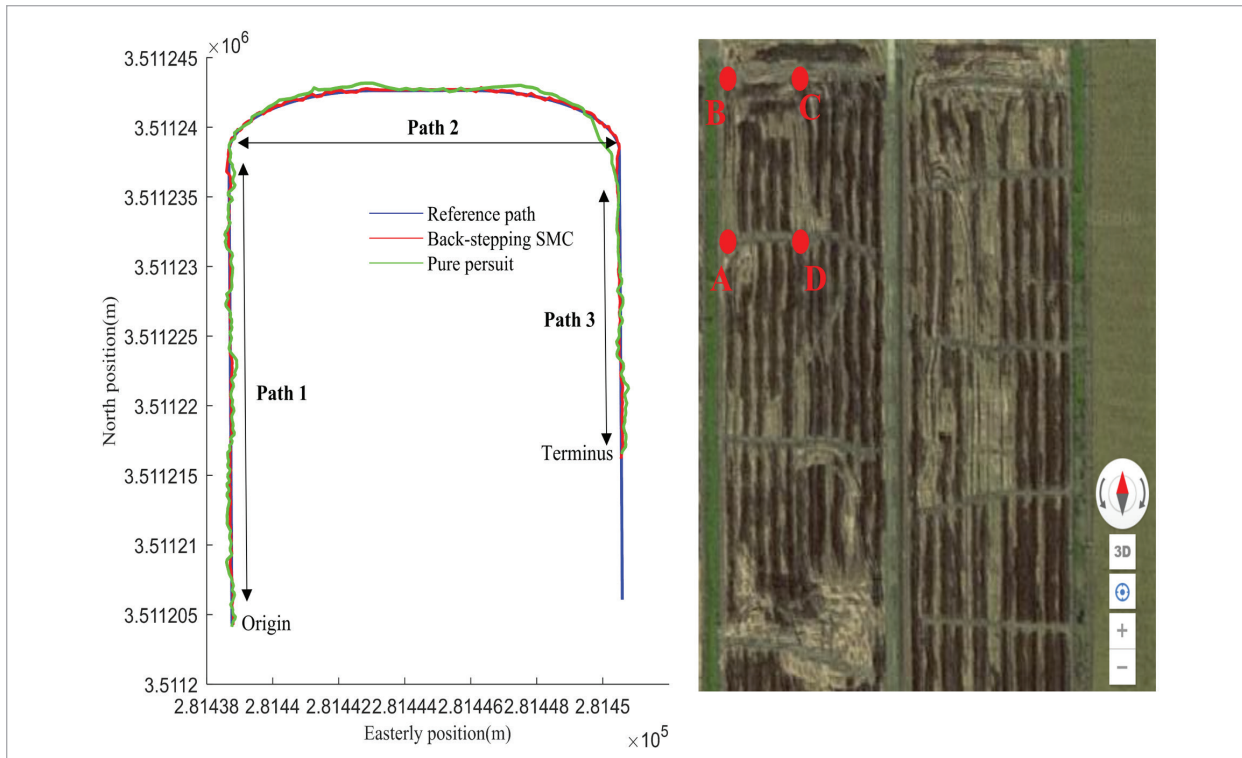


Figure 9
The actual lateral deviation under two different kinds of controllers

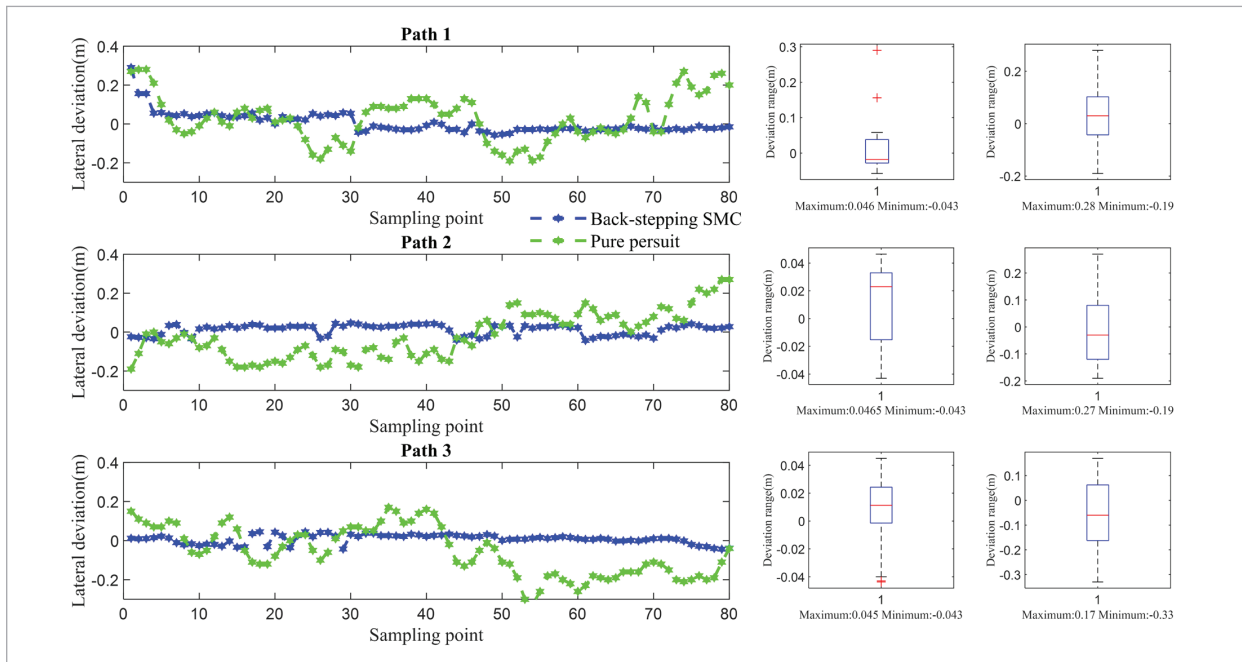


Table 2

The lateral deviation statistics under the backstepping-SMC control

The serial number of the path	Lateral deviation /m				
	Maximum value	Minimum value	Average value	root-mean-square	standard deviation
1	0.0460	-0.0430	0.0018	0.0528	0.0525
2	0.0465	-0.0430	0.0127	0.0266	0.0264
3	0.0450	-0.0430	0.0081	0.0232	0.0231

Table 3

The lateral deviation statistics under the fuzzy pure pursuit control

The serial number of the path	Lateral deviation /m				
	Maximum value	Minimum value	Average value	root-mean-square	standard deviation
1	0.2800	-0.1900	0.0300	0.1206	0.1199
2	0.2700	-0.1900	-0.0146	0.1213	0.1206
3	0.1700	-0.3300	-0.0560	0.1256	0.1248

6. Conclusions

In this paper, a back-stepping SMC is proposed for the unmanned tractors to realize the path following control with high robustness. Specifically, in this system, the time-varying parameters ESOs were used to estimate both the mismatched and matched disturbances; meanwhile, the bounded hyperbolic tangent function was used to limit the control input. The Lyapunov theory was applied to analyze the controller's stability, and the simulation and field experiments were carried out to verify its effectiveness. According to the experiment, the proposed controller can guar-

antee the lateral deviation within 0.045 m, verifying the effectiveness of the proposed back-stepping SMC for the unmanned farm tractor.

Acknowledgments

This research was funded by the “National Key Research and Development Program (2019YFB1312302)”, the “Key Research and Development Program of Jiangsu Province (BE2020327)”, and the “Key Research and Development Program of Jiangsu Province (BE2021313)”.

References

- Adams, B. T. Farm Machinery Automation for Tillage, Planting Cultivation, and Harvesting//Handbook of Farm, Dairy and Food Machinery Engineering. Academic Press, 2019, 115-131. <https://doi.org/10.1016/B978-0-12-814803-7.00005-1>
- Aghababa, M. P., Akbari, M. E. A Chattering-free Robust Adaptive Sliding Mode Controller for Synchronization of Two Different Chaotic Systems with Unknown Uncertainties and External Disturbances. Applied Mathematics and Computation, 2012, 218(9), 5757-5768. <https://doi.org/10.1016/j.amc.2011.11.080>
- Chen, C., Gao, H., Ding, L., Li, W., Yu, H., Deng, Z. Trajectory Tracking Control of WMRs with Lateral and Longitudinal Slippage Based on Active Disturbance Rejection Control. Robotics and Autonomous Systems, 2018, 107, 236-245. <https://doi.org/10.1016/j.robot.2018.06.011>

4. Ding, S., Li, S. Second-order Sliding Mode Controller Design Subject to Mismatched Term. *Automatica*, 2017, 77, 388-392. <https://doi.org/10.1016/j.automatica.2016.07.038>
5. Falcone, P., Borrelli, F., Asgari, J., Tseng, H. E., Hrovat, D. Predictive Active Steering Control for Autonomous Vehicle Systems. *IEEE Transactions on Control Systems Technology*, 2007, 15(3), 566-580. <https://doi.org/10.1109/TCST.2007.894653>
6. Fang, H., Fan, R., Thuilot, B., Martinet, P. Trajectory Tracking Control of Farm Vehicles in Presence of Sliding. *Robotics and Autonomous Systems*, 2006, 54(10), 828-839. <https://doi.org/10.1016/j.robot.2006.04.011>
7. Gao, Z. Scaling and Bandwidth-parameterization Based Controller Tuning. *ACC*, 2003.
8. Ginoya, D., Shendge, P. D., Phadke, S. B. Sliding Mode Control for Mismatched Uncertain Systems Using an Extended Disturbance Observer. *IEEE Transactions on Industrial Electronics*, 2013, 61(4), 1983-1992. <https://doi.org/10.1109/TIE.2013.2271597>
9. Han, J. From PID to Active Disturbance Rejection Control. *IEEE Transactions on Industrial Electronics*, 2009, 56(3), 900-906. <https://doi.org/10.1109/TIE.2008.2011621>
10. Ji, X., Wang, A., Wei, X. Precision Control of Spraying Quantity Based on Linear Active Disturbance Rejection Control Method. *Agriculture*, 2021, 11(8), 761. <https://doi.org/10.3390/agriculture11080761>
11. Oetiker, M. B., Baker, G. P., Guzzella, L. A Navigation-field-based Semi-autonomous Nonholonomic Vehicle-parking Assistant. *IEEE transactions on vehicular technology*, 2008, 58(3), 1106-1118. <https://doi.org/10.1109/TVT.2008.928643>
12. Perruquetti, W., Barbot, J. P. (Eds.). *Sliding Mode Control in Engineering*. Marcel Dekker, New York, 2002. <https://doi.org/10.1201/9780203910856>
13. Rubagotti, M., Estrada, A., Castaños, F., Ferrara, A., Fridman, L. Integral Sliding Mode Control for Nonlinear Systems with Matched and Unmatched Perturbations. *IEEE Transactions on Automatic Control*, 2011, 56(11), 2699-2704. <https://doi.org/10.1109/TAC.2011.2159420>
14. Utkin, V. I. *Sliding Modes in Control and Optimization*. Springer Science & Business Media, 2013.
15. Wang, H., Zuo, Z., Wang, Y., Yang, H., Chang, S. Composite Nonlinear Extended State Observer and Its Application to Unmanned Ground Vehicles. *Control Engineering Practice*, 2021, 109, 104731. <https://doi.org/10.1016/j.conengprac.2021.104731>
16. Wu, D., Zhang, Q., Reid, J. F. Adaptive Steering Controller Using a Kalman Estimator for Wheel-type Agricultural Tractors. *Robotica*, 2001, 19(5), 527-533. <https://doi.org/10.1017/S0263574701003459>
17. Wu, Y., Wang, L., Zhang, J., Li, F. Path Following Control of Autonomous Ground Vehicle Based on Nonsingular Terminal Sliding Mode and Active Disturbance Rejection Control. *IEEE Transactions on Vehicular Technology*, 2019, 68(7), 6379-6390. <https://doi.org/10.1109/TVT.2019.2916982>
18. Xia, Y., Pu, F., Li, S., Gao, Y. Lateral Path Tracking Control of Autonomous Land Vehicle Based on ADRC and Differential Flatness. *IEEE Transactions on Industrial Electronics*, 2016, 63(5), 3091-3099. <https://doi.org/10.1109/TIE.2016.2531021>
19. Xia, Y., Shi, P., Liu, G. P., Rees, D., Han, J. Active Disturbance Rejection Control for Uncertain Multivariable Systems with Time-delay. *IET Control Theory & Applications*, 2007, 1(1), 75-81. <https://doi.org/10.1049/iet-cta:20050138>
20. Xia, Y., Zhu, Z., Fu, M. Back-stepping Sliding Mode Control for Missile Systems Based on an Extended State Observer. *IET Control Theory & Applications*, 2011, 5(1), 93-102. <https://doi.org/10.1049/iet-cta.2009.0341>
21. Yao, L., Pitla, S. K., Zhao, C., Liew, C., Hu, D., Yang, Z. An Improved Fuzzy Logic Control Method for Path Tracking of an Autonomous Vehicle. *Transactions of the ASABE*, 2020, 63(6), 1895-1904. <https://doi.org/10.13031/trans.13737>
22. Yin, C., Sun, Q., Wu, J., Liu, C., Gao, J. Development of Electrohydraulic Steering Control System for Tractor Automatic Navigation. *Journal of Electrical and Computer Engineering*, 2018. <https://doi.org/10.1155/2018/5617253>
23. Yu, L., Yan, X., Kuang, Z., Chen, B., Zhao, Y.. Driverless Bus Path Tracking Based on Fuzzy Pure Pursuit Control with a Front Axle Reference. *Applied Sciences*, 2019, 10(1), 230. <https://doi.org/10.3390/app10010230>
24. Yu, S., Yu, X., Shirinzadeh, B., Man, Z. Continuous Finite-time Control for Robotic Manipulators with Terminal Sliding Mode. *Automatica*, 2005, 41(11), 1957-1964. <https://doi.org/10.1016/j.automatica.2005.07.001>
25. Zhang, Q., Reid, J. F., Noguchi, N. Agricultural vehicle navigation using multiple guidance sensors. In *Proceedings of the international conference on field and service robotics*, 1999.

26. Zhang, Y., Chen, Z., Zhang, X., Sun, Q., Sun, M. A novel control scheme for quadrotor UAV based upon active disturbance rejection control. *Aerospace Science and Technology*, 2018, 79: 601-609. <https://doi.org/10.1016/j.ast.2018.06.017>
27. Zheng, Q., Chen, Z., Gao, Z. A practical approach to disturbance decoupling control. *Control engineering practice*, 2009, 17(9): 1016-1025. <https://doi.org/10.1016/j.conengprac.2009.03.005>
28. Zhu, Q., Chen, W., Hu, H., Wu, X., Xiao, C., Song, X. Multi-sensor Based Attitude Prediction for Agricultural Vehicles. *Computers and Electronics in Agriculture*, 2019, 156, 24-32. <https://doi.org/10.1016/j.compag.2018.11.008>



This article is an Open Access article distributed under the terms and conditions of the Creative Commons Attribution 4.0 (CC BY 4.0) License (<http://creativecommons.org/licenses/by/4.0/>).